Optical and Quantum Electronics (2023) 55:1013
https://doi.org/10.1007/s11082-023-05259-w

Insight into the spin-polarized structural, optoelectronic, magnetic, thermodynamic, and thermoelectric properties of $PdBO_2$ (B = Al, Cr, and Rh) Delafossite semiconductor

Mohammed Elamin Ketfi[1] · Saber Saad Essaoud[2,3] · Said Al Azar[4] · Anas Y. Al-Reyahi[5] · Ahmad A. Mousa[6,7] · Ahmad Mufleh[8]

Received: 12 May 2023 / Accepted: 1 August 2023

Abstract
In this work, we performed first-principles calculations based on density functional theory and the semi-classical Boltzmann method to investigate the structural, optoelectronic, magnetic, thermodynamic and thermoelectric properties of $PdAlO_2$, $PdCrO_2$ and $PdRhO_2$ in the Tetragonal phase. Our calculations have revealed that these three compounds have indirect band gaps in the range of 2.14 to 2.68 eV. The thermodynamic properties are investigated using the quasi-harmonic model, where heat capacities at constant pressure and volume, entropy, Debye temperature, and thermal expansion coefficient are analyzed and discussed under both pressure and temperature effects. As a result of this study, $PdAlO_2$, $PdCrO_2$, and $PdRhO_2$ are promising materials for optoelectronic devices, especially photovoltaic materials in solar cells. In doing so, we computed for each compound the Seebeck coefficient, electrical conductivity, electronic thermal conductivity, and figure of merit in the temperature range from 300 to 500 K. The relaxation time and lattice thermal conductivity are calculated as well. Our results reveal that low thermal conductivity and a high Seebeck coefficient can be achieved at the same time. In addition, they exhibit a higher Seebeck for $PdAlO_2$ compared to $PdBO_2$ (B = Cr and Rh) up to 1.6 mV/K for $PdAlO_2$ at 300 K. Thereby improving their thermoelectric performance which makes them attractive thermoelectric materials at high temperatures.

Keywords Delafossite · TB-mBJ · Seebeck coefficient · Electrical and thermal conductivity coefficients · Dielectric function · Thermal expansion coefficient

1 Introduction

Delafossite class of oxides that was first discovered in 1965 and it represents a family of ternary compounds with the general formula ABO_2, where A, and B are metallic elements. The most common Delafossite is $CuAlO_2$, which is a p-type semiconductor with high electrical conductivity and transparency in the visible and near-infrared regions of the spectrum (Gillispie 2006; Shi et al. 2008; Chadwick et al. 2010).

Extended author information available on the last page of the article

The unique properties of Delafossites make them promising materials for a wide range of applications, including in electronic devices, energy storage and conversion, and optoelectronics. Delafossites are a class of materials that have recently gained attention due to their interesting electronic, magnetic, and optical properties (Woods-Robinson et al. 2020; Abdelhamid 2015). As a result, researchers have been studying these materials to better understand their fundamental properties and to explore their potential applications. Delafossite materials possess excellent high electrical conductivity, which makes them promising materials for use in electronic devices. Some Delafossites have been found to exhibit magnetic properties, which could have applications in magnetic data storage and other areas. Some Delafossites compounds have interesting optical properties, such as high transparency in the visible and near-infrared regions of the spectrum, which makes them potential candidates for use in solar cells and other optoelectronic devices. Moreover, they are known to have high thermal conductivity, which could have applications in thermal management for electronic devices (Akin et al. 2019).

Delafossite semiconductors exhibit a range of interesting physical and electronic properties, including high electrical conductivity, transparency in the visible region, and strong light absorption in the ultraviolet and blue regions of the spectrum. They also have high carrier mobility, which makes them promising candidates for use in high-speed electronic devices. Some of the potential applications of Delafossite semiconductors include transparent electrodes, photovoltaics, light-emitting diodes, and high-power electronics (Moreira et al. 2022). Their properties also make them attractive for use in other areas such as catalysis, sensing, and energy storage.

Some theoretical investigations of Delafossites have focused on understanding their electronic and magnetic properties. Density functional theory (DFT) calculations have shown that Delafossites have a range of electronic band structures, ranging from metals to semiconductors depending on the specific A and B ions used. Additionally, DFT calculations have predicted that some Delafossites, such as $CuCrO_2$ and $CuFeO_2$ (Akin et al. 2019; Moreira et al. 2022), exhibit antiferromagnetic ordering due to the coupling of spins on the transition metal ions. Also, an ab initio study carried out by Ali et al. (2015) demonstrated the semiconductive behavior of $CuXO_2$ compounds (X = Al, Ga, In, B, La, Sc, Y).

Experimental studies of Delafossites included the electronic and optical properties of one of the most well-known Delafossites is $CuAlO_2$, where this oxide appears high electrical conductivity and optical transparency (Zhang et al. 2019). $CuAlO_2$ has high carrier mobility and low carrier concentration, making it an excellent candidate for transparent conductive electrodes in optoelectronic devices. Additionally, Delafossites have been studied for their photovoltaic properties, with $CuInO_2$ and $CuGaO_2$ both showing promising results for solar cell applications. $PdRhO_2$ compound was treated experimentally by Kushwaha et al. (2017), where it was found to crystallize in a rhombohedral type structure, where the dimensions of the crystal cell were a = 3.0240 Å and c = 18.096 Å.

The use of semiconductors in electronic devices relies on the characteristics and value of their energy gap. Direct bandgap semiconductors possess a high likelihood of direct electron transitions between energy bands, resulting in efficient emission and absorption of light. Consequently, these semiconductors find extensive applications in fiber-optic communication, photovoltaic cells, and technologies that demand efficient light emission, including the production of bright LED lights and lasers used in displays, lighting, and telecommunications. They excel at converting electrical energy into light with remarkable efficiency. On the other hand, indirect semiconductors have limited effectiveness in applications reliant on light emission and absorption (Sâad-Essaoud et al. 2023a). However, they hold great significance in electronic devices such as transistors and thermoelectric

devices. Due to the high demand for both types of semiconductors, these reasons motivated us to search for these properties in some Delafossite compounds that had not been studied before.

2 Computational details

In this paper, the Full-Potential Linearized Augmented Plane Wave (FP-LAPW) method is used within the WIEN2k code (Blaha et al. 2020) to predict the structural, optoelectronic, and thermodynamic properties of $PdAlO_2$, $PdCrO_2$, and $PdRhO_2$ based on density functional theory (DFT). The revised Perdew-Burke-Ernzerhof (PBE) parameterization of the generalized gradient approximation (Perdew et al. 1996) (GGA) is used as an exchange–correlation functional for structural properties, while the modified Becke-Johnson exchange potential (Becke and Johnson 2006) is used for optoelectronic properties. The procedure entails partitioning the unit cell into a set of spherical, non-overlapping muffin tins and interstitial space. To obtain energy eigenvalue convergence, the wave function in interstitial regions was enlarged in plane wave with a cut-off of $R_{MT} \times K_{MAX} = 8$, where R_{MT} is a minimal muffin-tin radius and K_{MAX} is the magnitude of the maximal K vector wave in the Brillouin zone. Spheres with angular momentum up to $l_{max} = 10$ use spherical harmonic expansion. The interstitial wave function is plane wave expanded, whereas the spheres employ spherical harmonic expansion. For Pd, Al, Cr, Rh, and O atoms, muffin-tin radius R_{MT} is 2.3, 1.8, 2.0, 2.2, and 1.6 (a.u). Valence electron configurations and core-valence separation are given. Pd ($4d^{10}$), Al ($3s^2\ 3p^1$), Cr ($3d^5\ 4s^1$), Rh ($4d^8\ 5s^1$), and O ($2s^2\ 2p^4$) have valence electron electronic configurations for Brillouin zone (BZ) integration. We used 6 eV to discriminate valence and core states. We also set charge convergence to 10^{-3} and convergence energy to 10^{-5}. The GIBBS2 code employs the quasi-harmonic model (Otero-de-la-Roza and Luaña 2011; Otero-de-la-Roza et al. 2011) to consider the influence of pressure and temperature on various thermal properties. Meanwhile, the estimation of thermoelectric properties is carried out using the semi-local Boltzmann transport theory, which is implemented in the BoltzTraP code (Madsen and Singh 2006).

3 Results and discussion

3.1 Structural and magnetic properties

Delafossites have attracted significant attention due to their interesting electronic, optical, and magnetic properties, which make them promising candidates for a wide range of applications such as transparent conductive electrodes, photovoltaic, and spintronic. For this reason, we studied $PdBO_2$ (B = Al, Cr and Rh) compound in tetragonal phase structure with R-3m space group (166) as shown in Fig. 1 (a and b). Before calculating lattice constants, bulk modulus, and cohesive energy, we must determine the positions of the atoms that make up these compounds through full geometry optimizations. The internal positions of atoms have been relaxed via the total energy and force minimization system based on Broyden's approach (Broyden 1970a, 1970b), which yields an appropriate relaxed structure if the force applied to each atom is under 0.001 Ry/Å. Table 1 compares GGA-optimized atom locations for each elements to theoretical values. Computing the total energy for various volumes by applying the Murnaghan equation of state (Murnaghan 1944) to obtain the

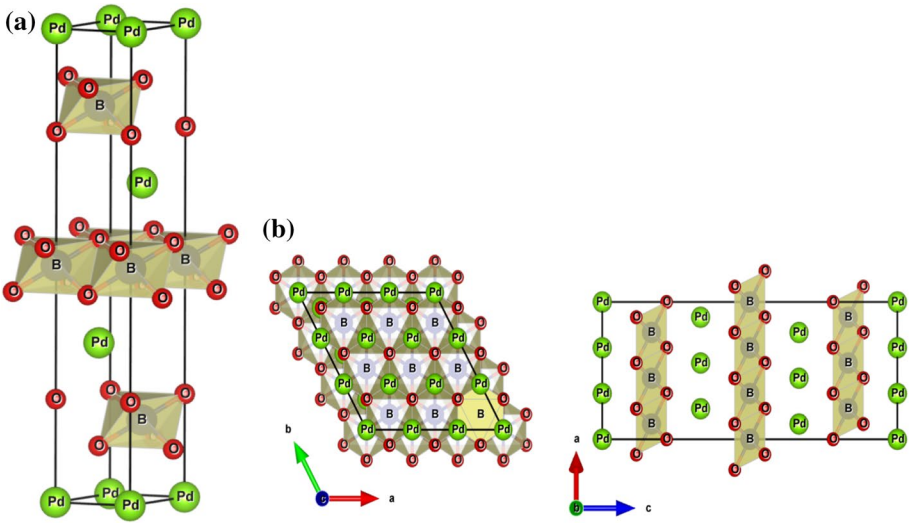

Fig. 1 **a** Crystal Tetragonal structure of $PdBO_2$ (B = Al, Cr and Rh) compounds. **b** Polyhedral view along b and c-axis

Table 1 The atomic positions were calculated using PBE approximations of $PdBO_2$ (B = Al, Cr and Rh) compounds

Materials	Atoms	GGA			Other work (Shi et al. 2017)		
		x	y	z	x	y	z
$PdAlO_2$ (R-3m # 166)	Pd	0.0000	0.0000	0.0000	0.0000	0.0000	0.5000
	Al	0.5000	0.5000	0.5000	0.0000	0.0000	0.0000
	O	0.7790	0. 7790	0. 7790	0.0000	0.0000	− 0.38662
	O	0.2210	0.2210	0.2210	–	–	–
$PdCrO_2$ (R-3m # 166)	Pd	0.0000	0.0000	0.0000	0.0000	0.0000	0.5000
	Cr	0.5000	0.5000	0.5000	0.0000	0.0000	0.0000
	O	0.7821	0.7821	0.7821	0.0000	0.0000	− 0.38882
	O	0.2179	0.2179	0.2179	–	–	–
$PdRhO_2$ (R-3m # 166)	Pd	0.0000	0.0000	0.0000	0.0000	0.0000	0.0000
	Rh	0.5000	0.5000	0.5000	0.0000	0.0000	0.5000
	O	0.7788	0.7788	0.7788	0.0000	0.0000	0.11048
	O	0.2212	0.2212	0.2212	–	–	–

volume with the lowest energy yields each unit cell's lattice parameter "*a*" After that, the total energy for different c/a ratios in the tetragonal structure at a fixed volume is estimated to calculate the lattice constant "c" for all three compounds $PdAlO_2$, $PdCrO_2$, and $PdRhO_2$ in the same phase.

Table 2 summarizes the results and compares them to other accessible data; the table demonstrates that the GGA approximation yields satisfactory outcomes for the three compounds $PdAlO_2$, $PdCrO_2$ and $PdRhO_2$. Bulk modulus B(GPa) characterizes the

Table 2 The calculated equilibrium lattice constants, bulk modulus, and cohesive energy for $PdBO_2$ (B = Al, Cr and Rh) compounds obtained by using GGA-PBE approximations

	a (Å)	c(Å)	B(GPa)	E_{coh} (eV/atom)
$PdAlO_2$				
GGA	2.8233	17.8289	191.4320	5.56
Theo (Shi et al. 2017)	2.8607	18.0958	–	–
$PdCrO_2$				
GGA	2.9367	18.2625	189.9776	6.34
Theo (Shi et al. 2017)	3.0090	18.2310	–	–
$PdRhO_2$				
GGA	3.0379	18.0388	209.5582	4.63
Theo (Shi et al. 2017)	3.0830	18.3068	–	–
Exp (Kushwaha et al. 2017)	3.0240	18.0960		

resistance of a material to hydrostatic pressure-induced deformation. Thus, the $PdRhO_2$ combination is more resistant to external pressure due to the quantity and strength of its bonds between atoms. This result can be confirmed by using the following formula to calculate the cohesive energy of the compounds.

$$E_{coh} = \frac{(E^{Pd}_{atom} + E^{B}_{atom} + 2\,E^{O}_{atom}) - E^{PdBO_2}_{tot}}{N_{Pd} + N_B + N_O} \tag{1}$$

$E^{PdBO_2}_{tot}$ is the bulk $PdBO_2$ compound's energy, where N_{Pd}, N_B, and N_O are the numbers of Pd, B, and O atoms in the unit cell and E^{Pd}_{atom}, E^{B}_{atom} and E^{O}_{atom} are their isolated atom energies. The second compound has the greatest cohesive energy and is highly structurally stable.

ABO_2 is a Delafossite oxide compound that exhibits a variety of interesting magnetic properties. Previous studies have shown that ABO_2 can exhibit ferromagnetism, antiferromagnetism, or spin glass behavior depending on the specific A and B cations present in the crystal structure. According to Fig. 2, we can easily see that the ferromagnetic state has lower energy than paramagnetic state, and thus the three studied compounds are more stable in the ferromagnetic state. Our aim here is to investigate how the three compounds' magnetic stability is affected by pressure, which can result in either compression or expansion of the unit cell, consequently leading to a decrease or increase in the lattice constant.

In Fig. 3, we have illustrated the alterations in the total and partial magnetic moments of the atoms concerning the volume. Notably, the magnetic moment of $PdBO_2$ (B = Al, Cr) remains unchanged despite the volume change, as shown by the horizontal straight line. Furthermore, the magnetic moment of the Chrome atom exhibits a significant increase with a rise in volume, unlike those of Palladium, Rhodium, Oxygen atoms, and the interstitial zone, which display stable magnetic moment values with a rise in volume. These results substantiate the magnetic stability of the three examined compounds under varying pressure conditions.

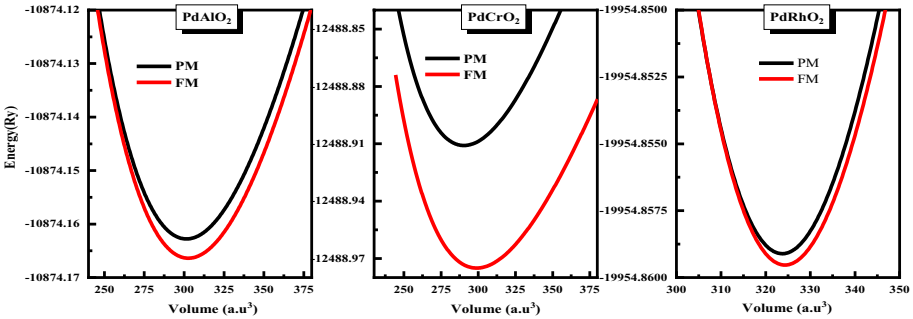

Fig. 2 The total energy as function of the unit cell volume of $PdBO_2$ (B = Al, Cr, and Rh) compounds in paramagnetic and ferromagnetic states

3.2 Electronic properties

Delafossite oxides have potential applications in a wide range of fields such as energy conversion, catalysis, and electronic devices. The study of electronic properties is crucial for understanding and optimizing the properties and performance of Delafossite oxides, and for developing new applications for these materials.

The energy band structure of the three materials under investigation was computed at the high-symmetry points within the first Brillouin zone. Figure 4 illustrates that the three compounds exhibit distinct behavior. Notably, both $PdAlO_2$ and $PdRhO_2$ demonstrate semiconducting characteristics in the spin-up state, featuring indirect energy gaps of 2.28 eV (Γ-L) and 2.14 eV (Γ-H) respectively. Conversely, they exhibit metallic behavior in the spin-down state. On the other hand, the compound $PdCrO_2$ displays metallic behavior in the spin-up state, while in the spin-down state; it behaves as a semiconductor with an estimated indirect energy gap of 2.68 eV (Γ-M).

The densities of states were computed using the TB-mBJ approach and afterwards plotted in Fig. 5.The studied compounds show two bands (conduction higher than Fermi level and valence below) separated by an indirect gap, where the band gaps calculated via TB-mBJ approximation are 2.28, 2.68, and 2.14 eV for $PdAlO_2$, $PdCrO_2$, and $PdRhO_2$,

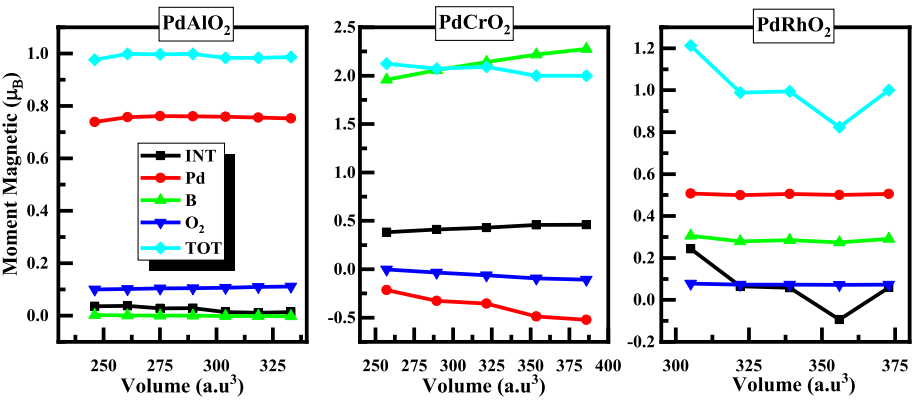

Fig. 3 Total and partial magnetic moment variations as function of volume for $PdBO_2$ (B = Al, Cr and Rh)

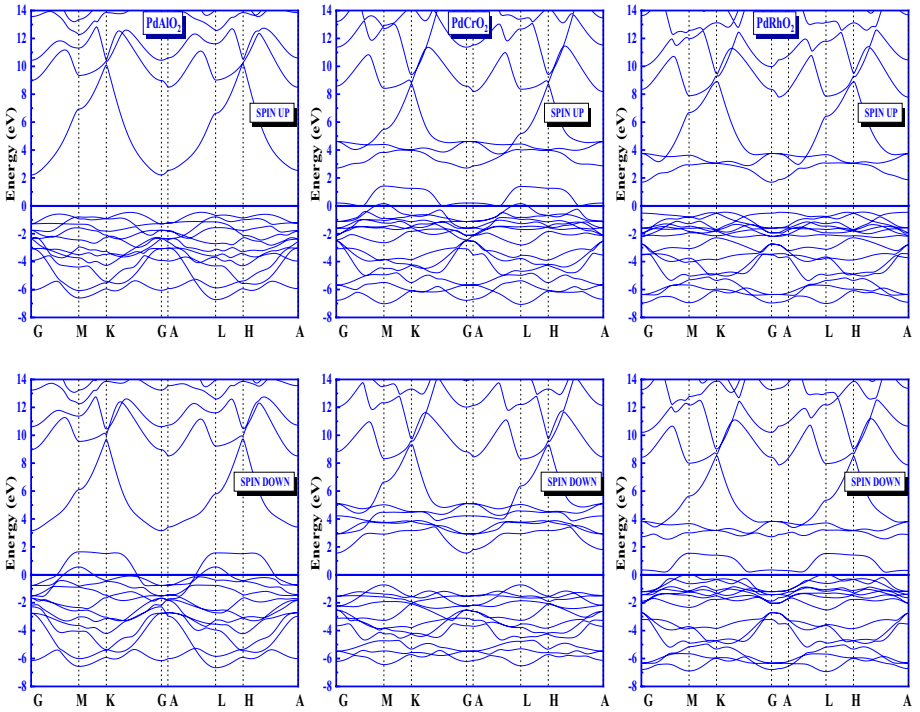

Fig. 4 Band structure curves for $PdBO_2$ (B = Al, Cr and Rh) within the TB-mBJ approximation

respectively, and our results are in excellent agreement with the other works (Shi et al. 2017). The three compounds investigated in our work were having band gaps in one spin direction, confirming the existence of two bands. In the spin-up direction, both $PdAlO_2$ and $PdRhO_2$ compounds show an overlap among both conduction and valence bands, implying metallic behavior. In the spin-down direction, $PdRhO_2$ has an indirect band gap of 2.14 eV.

To figure out how each band in a band structure spectrum is made, we look at Fig. 5's total and partial density of states for the atomic orbitals. These compounds tend to be semiconductors because there is no state density near the Fermi level. For the three compounds $PdBO_2$ (B = Al, Cr, and Rh) in the tetragonal phase structure, the conduction band originates mainly via the dominant contribution of the Palladium atom's "d" orbitals, with a weak contribution from each of Pd's "s" and "p" orbitals. This is in contrast to the "s" and "p" orbitals of the Al and O atoms, which indicate a strong hybridizing in the range of −7 eV to 0 eV.

3.3 Optical properties

Delafossite compounds exhibit a variety of interesting optical properties, which make them useful in various applications such as catalysis, photocatalysis, and optoelectronics. One of the most important optical properties of ABO_2 compounds is their bandgap energy, which determines their ability to absorb light and their optical transparency. The bandgap energy

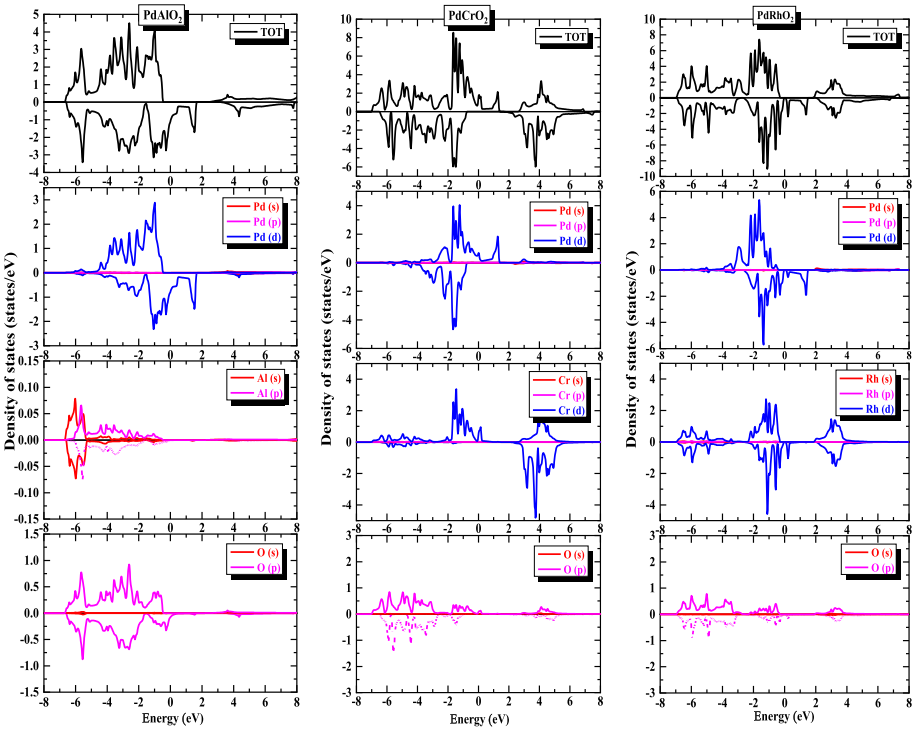

Fig. 5 The calculated total and partial density of states for $PdBO_2$ (B = Al, Cr and Rh) within the TB-mBJ approximation

of ABO_2 compounds can be tuned by varying the composition and crystal structure, making them useful for a range of applications. Another important optical is their luminescence behavior. Many ABO_2 compounds exhibit luminescence due to the presence of defect states in their crystal structure, which can be excited by light and emit light at different wavelengths. This property has been exploited in various applications such as solid-state lighting and fluorescent probes (Singh et al. 2018; Hanaor and Sorrell 2011; Zhang et al. 2018).

We used the dielectric complex function ε(ω) to examine the real $\varepsilon_1(\omega)$ and imaginary $\varepsilon_2(\omega)$ parts, which are determined by the formula (Khan et al. 1993; Kataria et al. 2022; Ambrosch-Draxl and Sofo 2004; Gajdoš et al. 2006):

$$\varepsilon(\omega) = \varepsilon_1(\omega) + i\varepsilon_2(\omega) \tag{2}$$

The real part of the dielectric function $\varepsilon_1(\omega)$ presents the dispersion of the incident photons by the substance's parts (Ul Haq et al. 2020) and it gives us more information about the electronic polarizability state of the material (Sâad-Essaoud et al. 2023b) while the imaginary part of the dielectric function $\varepsilon_2(\omega)$ means the energy absorbed by the material. The imaginary part $\varepsilon_2(\omega)$ is estimated using the electronic band structure by relating the momentum matrix elements between the occupied and unoccupied electronic states whereas the real part can be obtained from $\varepsilon_2(\omega)$ using the Kramers–Kronig transformation (Telfah et al. 2021).

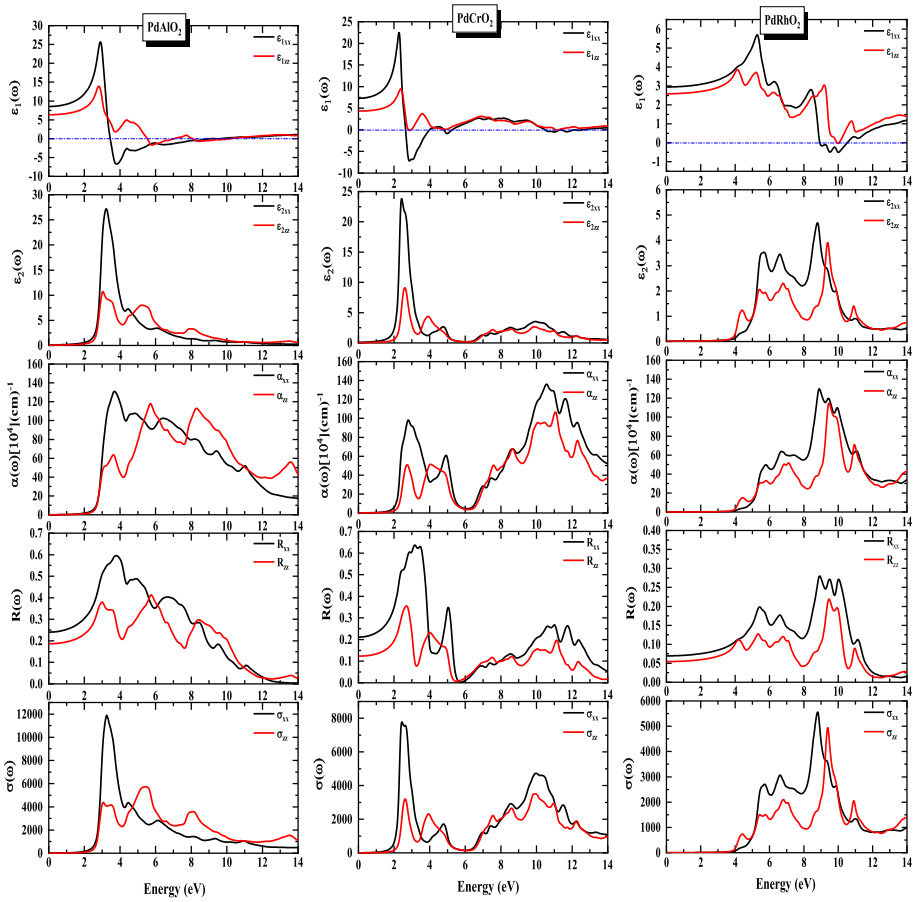

Fig. 6 Optical properties of $PdBO_2$ (B = Al, Cr and Rh) within TB-mBJ approach

Figure 6 shows the calculated real and imaginary components of the examined compounds' dielectric functions along the x, y, and z directions using the TB-mBJ approximation. Through this figure, we can observe that the computed static dielectric constant values (the real dielectrics at zero frequency $\varepsilon_1(0)$) show that $PdAlO_2$ has a greater value than the other compounds. In contrast to the absorption coefficient, which is available in this energy range, the spectrum of $\varepsilon_1(\omega)$ increases sharply from the static dielectric constant $\varepsilon_1(0)$ and reaches its maximum value at an energy equal to 2.52, 2.26, and 5.8 eV for $PdAlO_2$, $PdCrO_2$, and $PdRhO_2$, respectively. However, since it gradually decreases to take negative values in the range of 3–12 eV for all the studied compounds, where their behavior in this region turns to metallic.

Regarding the spectra of the imaginary portion $\varepsilon_2(\omega)$ plotted in Fig. 6, we can observe that the optical band gaps for $PdAlO_2$, $PdCrO_2$, and $PdRhO_2$ are 2.5, 2.1, and 3.8 eV, respectively, as derived from the imaginary part of the dielectric function using the TB-mBJ approximation. The $\varepsilon_2(\omega)$ spectra represent the absorption that may result from electronic excitation from valence states below the Fermi level in the conduction states, and we can note from the spectra that this absorption is only possible if the incident photons have an energy value higher than the energy gap.

The absorption coefficient α(ω) is connected to the extinction coefficient k(ω), by the following formula (Al-Reyahi et al. 2023):

$$\alpha(\omega) = (4\pi/\lambda)\mathrm{k}(\omega) \tag{3}$$

where λ is the wavelength of light in the vacuum which is calculated via the dielectric function by the following relationship (Sâad Essaoud et al. 2022):

$$\alpha(\omega) = \frac{2\pi\omega}{c}\sqrt{\frac{-R_e(\varepsilon(\omega)|\varepsilon(\omega)|)}{2}} \tag{4}$$

The absorption edge is located at around 2.28 eV for $PdAlO_2$, 2.68 eV for $PdCrO_2$ and 2.14 eV for $PdRhO_2$. All three compounds respond well in the range of 3.6 to 20 eV for $PdAlO_2$, 2.7 to 47 eV for $PdCrO_2$ and 5.5 to 20 eV for $PdRhO_2$ to incident photons.

We define another parameter, which is the reflective coefficient R(ω). It characterizes the part of the reflected energy from the surface of the solid and can be derived from the refractive index (Sâad Essaoud et al. 2022) as follows:

$$R(\omega) = \left|\frac{(n(\omega)-1)^2 + k(\omega)^2}{(n(\omega)+1)^2 + k(\omega)^2}\right| \tag{5}$$

Figure 6 shows that the zero-frequency reflectivity limit of $PdBO_2$ is found to be 24% for $PdAlO_2$, 21% for $PdCrO_2$ and 7% for $PdRhO_2$. High reflex peaks are observed at energies 3.9, 3.1 and 8.9 eV for the three compounds corresponding to the negative values of $\varepsilon_1(\omega)$.

The following formula defined optical conductivity (Sâad-Essaoud et al. 2023c):

$$\sigma(\omega) = -(i\omega/4\pi)\varepsilon(\omega) \tag{6}$$

Figure 6 shows that the optical conductivity starting from 2.28 eV, 2.68 eV and 2.14 eV for $PdAlO_2$, $PdCrO_2$ and $PdRhO_2$ respectively. As remark, the maximum of optical conductivity of the compounds is at 3.2 eV for $PdAlO_2$, 2.4 eV for $PdCrO_2$ and 8.8 eV for $PdRhO_2$.

3.4 Thermodynamic properties

In order to achieve optimal efficiency for materials utilized in solar energy systems, a comprehensive understanding of their properties is imperative. This includes an awareness of how their properties are affected by temperature and pressure changes. The ability of materials to change their energy absorption capacity, their coefficient of thermal expansion, their resistance to deformation, and other qualities are crucial to investigate.

Theoretical exploration of these characteristics was carried out within a temperature span of 1000 units and under the influence of pressure up to 30 GPa using the quasi-harmonic Debye model, which was applied in the GIBBS2 code (Otero-de-la-Roza and Luaña 2011; Otero-de-la-Roza et al. 2011).

The Gibbs free energy expression is employed for investigating changes in the thermodynamic properties of a solid material induced by temperature and pressure.

$$G^*(\mathrm{x},\mathrm{V};\mathrm{P},\mathrm{T}) = \mathrm{E}_{\mathrm{stat}}(\mathrm{x},\mathrm{V}) + \mathrm{PV} + \mathrm{A}^*_{\mathrm{vib}}(\mathrm{x},\mathrm{V};\mathrm{T}) + \mathrm{F}^*_{\mathrm{el}}(\mathrm{x},\mathrm{V};\mathrm{T}) \tag{7}$$

where A^*_{vib} and F^*_{el} are the respective non-equilibrium vibrational Helmholtz free energies and electronic free energies, PV stands for the hydrostatic condition, E_{stat} is the total energy. The non-equilibrium vibrational Helmholtz free energy, A^*_{vib}, can be expressed using Debye's model in terms of the density of phonon states (the vibrational density of states), g(ω):

$$A^*_{vib} = \int_0^\infty \left[\frac{\omega}{2} + k_B T \, Ln(1 - e^{-\frac{\omega}{k_B T}})\right] g(\omega) d\omega \tag{8}$$

$$F^*(x, V; T) = E_{stat}(x, V) + A^*_{vib}(x, V; T) \tag{9}$$

D (θ/T) stands for the Debye integral, and n denotes the number of atoms per unit volume. This expression is represented as:

$$D(x) = \frac{3}{x^3} \int_0^x \frac{y^3 e^{-y}}{1-e^{-y}} dy \tag{10}$$

At constant pressure and temperature, we minimize the Gibbs free energy G* with respect to volume to obtain the equilibrium state.

$$\left(\frac{\partial G^*(V, P, T)}{\partial V}\right)_{P,T} = 0 \tag{11}$$

In order to get the formulas for various thermal quantities, such as entropy (S), the heat capacity at constant volume (Cv), and the coefficient of thermal expansion (α), we must first solve the last equation.

$$S = -3nk_B \ln(1 - e^{-\theta_D/T}) + 4nk_B D(\theta_D/T) \tag{12}$$

$$C_v = 12nk_B D(\theta_D/T) - \frac{9nk_B \theta_D/T}{e^{\theta_D/T} - 1} \tag{13}$$

$$\alpha = -\frac{1}{V}\left(\frac{\partial V}{\partial T}\right)_P = \frac{\gamma C_V}{V B_T} \tag{14}$$

The heat capacity at volume constant C_v, which is represented by the formula (13) shows how much energy of one mole of a substance can absorb when the temperature rises by 1.0 K. We displayed the fluctuation of $PdBO_2$'s heat capacity (B = Al, Cr, and Rh) as a function of temperature in Fig. 7. Figure 7 illustrates how C_v increases with temperature in exponential proportions (~T^3) at low temperatures (less than 200 K), but sets up 100 J/molK at temperatures equal to or more than 450 K, which is in conformity with the Petit-Dulong law (Petit and Dulong 1819).

In Fig. 7, we presented a plot of the thermal quantity, entropy, which signifies the irretrievable energy in a system. The results show that $PdRhO_2$ has a greater entropy value compared to the other compounds. Additionally, the three entropy curves demonstrate a quasi-linear increase with increasing pressure and temperature independently. This observation can be explained by the fact that an increase in temperature leads to a rise in

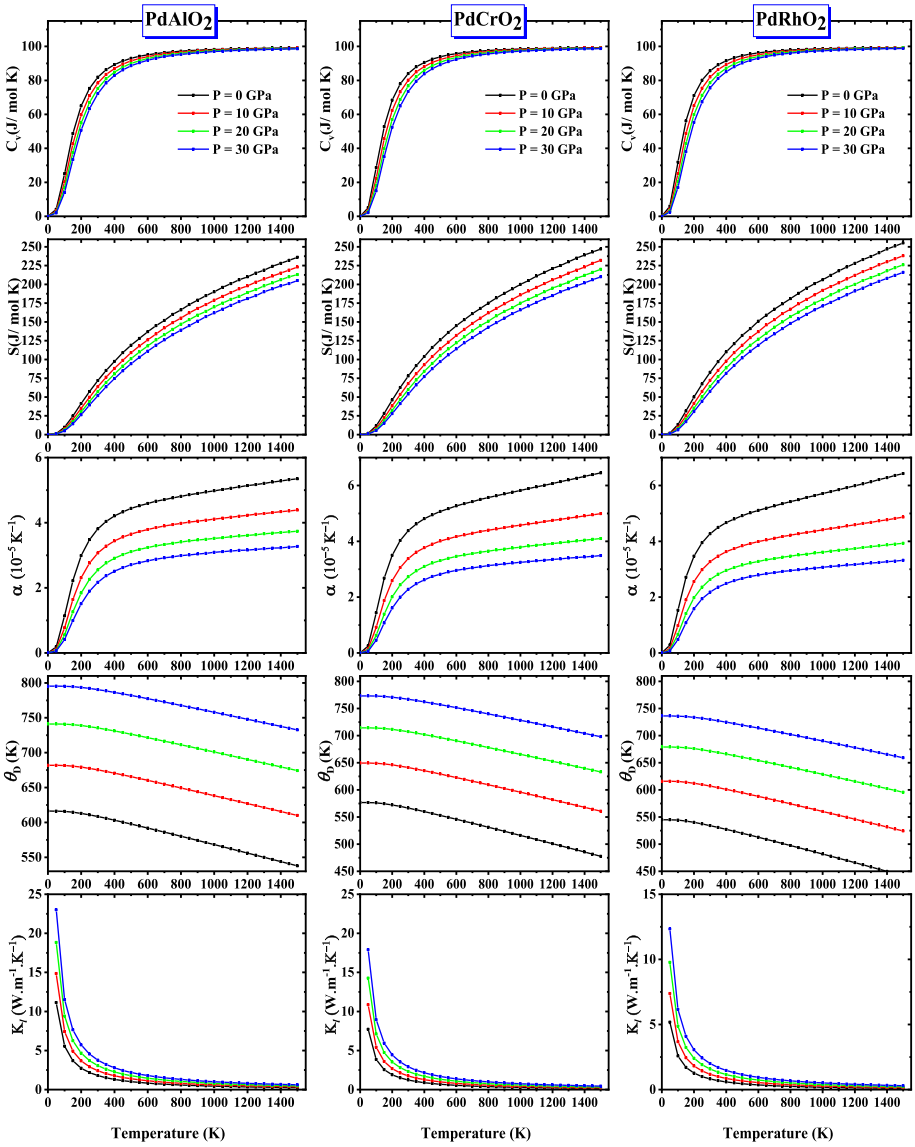

Fig. 7 Heat capacity (C_V), entropy (S), thermal expansion (α), Debye temperature (θ_D), and crystal conductivity (κ_l) of $PdBO_2$(B = Al, Cr, and Rh) Delafossite compounds vary with temperature and pressure

vibrational modes, which, in turn, increases the number of possible configurations. Conversely, an increase in pressure affects atomic movement, ultimately reducing vibrations.

The fraction of a substance's volume change as the temperature varies is expressed by thermal expansion. A change in the substance's volume results from increased atom mobility brought on by a rise in temperature. The nature of its atoms, the number of bonds, and the kind of its structure are the three most significant variables that affect α

(Otero-de-la-Roza and Luaña 2011). The fluctuation of α as a function of temperature is depicted in Fig. 7.

This portion of the chart shows that all compounds under study exhibit rapid temperature increases for temperatures under 200 K and gradual temperature increases for temperatures more than or equal to 200 K. Additionally, we can see that the $PdCrO_2$ compound has the highest α at temperatures below 350 K, and the same compound has a greater thermal expansion value than the other at temperatures above 350 K. Debye temperature (θ_D) helps to know many properties of solids like melting temperature, specific heat etc., directly or indirectly (Ali et al. 2020). It is the most significant thermal attribute. It represents the temperature that produced the most vibrational modes and is linked to a variety of mechanical and elastic properties (Sâad-Essaoud et al. 2023c). Figure 7 shows the calculated results for the temperature dependence of θ_D for all compounds $PdBO_2$ (B = Al, Cr, and Rh). When the temperature is raised, θ_D linearly decreases, with $PdAlO_2$ having the greatest value among the $PdCrO_2$ and $PdRhO_2$ compounds.

We looked at Fig. 7's temperature-dependent changes in the crystal thermal conductivity κ_l for $PdBO_2$ (B = Al, Cr, and Rh) in order to determine the distribution of phonon contributions to thermal conductivity. The Slack model formula can be used to compute the κ_l (Slack 1973):

$$K_l = \frac{A\vartheta_D^3 V^{1/3} m}{\gamma^2 n^{2/3} T} \tag{15}$$

where A is a physical constant equal to $A = \frac{2.4310^{-8}}{1-\frac{0.514}{\gamma}+\frac{0.228}{\gamma^2}}$ and ϑ_D, γ, V, n and m are the Debye temperature, Grüneision parameter, the volume per atom, the number of atoms in the primitive unit cell and m is the average mass of all the atoms in the crystal respectively. The crystal thermal conductivity of the three studied compounds under the influence of temperature as well as at different pressures showed that the vibrating atoms in the crystal lattice have a significant contribution to the transfer of thermal energy at low temperatures (less than 100 K), and it is directly proportional to the increase in pressure, and its value for the compound $PdAlO_2$ is greater than the two other compounds at the same temperature and pressure. Figure 7 shows that κ_l for $PdBO_2$ (B = Al, Cr, and Rh) exponentially drops with increasing temperature and reaches its lowest point when the temperature is above 500K, however at lower temperatures the thermal conductivity of $PdAlO_2$ compound is significantly higher than that of the other compounds.

3.5 Thermoelectric properties

We depend on the semi-classical Boltzmann transport theory implemented in the BoltzTraP code (Becke and Johnson 2006) to estimate the Seebeck coefficient (S), electrical conductivity (σ/τ), electronic thermal conductivity (κ/τ), and electronic specific heat capacity (c) of $PdBO_2$ compounds (B = Al, Cr, and Rh) for different temperature (300, 400, and 500 k) in the first step.

The Seebeck coefficient intrinsic to a material represents the proportionality between the voltage generated across the material's ends, and the thermal gradient applied to it. When exposed to this gradient, the charge carriers, such as electrons or holes (Mousa et al. 2022), in the material become mobile and lead to the induction of an electric current.

For all $PdBO_2$ (B = Al, Cr, and Rh) compounds, the fluctuation of the Seebeck coefficient along the relative chemical potential to the Fermi level μ_0 was depicted in Fig. 8 at

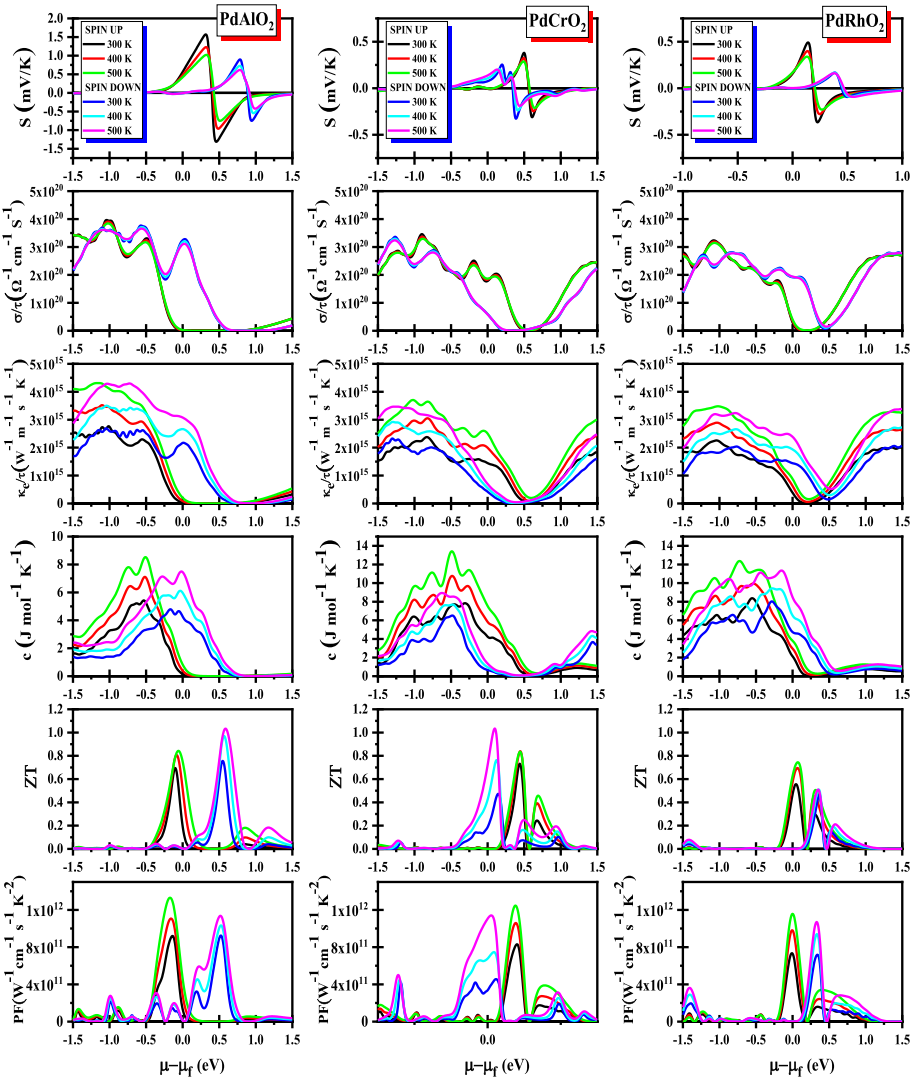

Fig. 8 Changes in the Seebeck coefficient (Cv), electrical conductivity (σ/τ), thermal conductivity (κ/τ), electronic specific heat capacity (c), figure of merit (ZT), and power factor (PF) for $PdBO_2$ compounds (B = Al, Cr, and Rh) for various temperature values (300, 400, and 500 K) as a function of the relative chemical potential

three different temperature levels (300, 400, and 500 K). The acquired data shows that for the three materials under study, the Seebeck coefficient is at its maximum at a temperature of 300 K. We can also see that the Seebeck coefficient of the $PdAlO_2$ molecule is substantially higher than that of the other two compounds, reaching a maximum value of 1.5 mV/K at 300 K and falling to 0.7 mV/K at 500 K.

When examining thermoelectric phenomena, three extra key parameters are extremely important. These characteristics include the material's electrical conductivity (σ/τ),

thermal conductivity (κ/τ), and electronic specific heat (*c*). These variables shed light on how the material's electrical conductivity, thermal conductivity, and heat capacity are affected by the mobility of electrons. Figure 8 illustrates the findings about the variations in electrical conductivity as a function of the relative chemical potential at various temperatures (300, 400, and 500 K). The electrical conductivity of the $PdRhO_2$ compound is high when the relative chemical potential is greater than the other studied compounds, whereas the electrical conductivity of the $PdAlO_2$ compound is higher when the relative chemical potential is lower. It can also be noted that the electrical conductivity has a maximum value at the temperature of 300 K and decreases slightly with increasing temperature for all the studied compounds.

The Wiedemann–Franz law establishes a direct correlation between the contributions of electrons to electrical and thermal conductivity. This law is expressed by the relation $\kappa = L\sigma T$, where κ refers to electronic thermal conductivity, σ is electrical conductivity, T is temperature, and L is the Lorentz constant. As a result, the curves representing the electronic thermal conductivity (κ/τ) and electrical conductivity (σ/τ) typically exhibit comparable shapes, as shown in Fig. 8.

The electron heat capacity is a way to quantify the role that free electrons play in the heat transport of solid materials (Ali et al. 2021a). Figure 8 illustrates how the electronic heat capacity (c) varies depending on the relative chemical potential at various temperatures (300, 400, and 500K) in both. The findings showed that for the three examined compounds, the value of electronic heat capacity (c) assumes higher values in the range of relative chemical potentials between -1.0 eV and 0 eV, and the value of the capacity rises with increasing temperature. $PdCrO_2$ has a higher electronic heat capacity (c) than the other compounds, in contrast to $PdAlO_2$, which has the lowest values, according to the displayed curves.

The figure of merit (ZT) factor for each compound is shown in Fig. 8 as a function of the chemical potential at various temperatures. This variable gauges a substance's capacity to transform heat into usable electric energy. As was already mentioned, different materials have different capacities for converting heat into electricity. Thermoelectric parameters such as the contribution of electrons to electrical and thermal conductivity and the Seebeck coefficient are linked to the material's figure of merit, which can be used to theoretically anticipate this change. A material needs to have a high Seebeck factor, high electrical conductivity, and low thermal conductivity in order to have a high ZT. In contrast to storing or conveying heat energy as heat, these qualities are necessary for efficiently converting heat energy into electricity. Figure 8 shows the ZT variation in terms of the chemical potential at various temperatures. It can be shown that $PdAlO_2$ and $PdCrO_2$ have higher ZT factors than $PdRhO_2$, which has a lower ZT.

The power factor ($PF = \frac{S^2\sigma}{\kappa}$) is a keynote parameter of transport properties (Ali et al. 2021b), The power factor of the three studied compounds showed an increase in its value with the increase in temperature in both cases of spin, and its value is high next to the Fermi level, which confirms that these compounds have high thermoelectric efficiency without the need doping with charge carriers.

4 Conclusion

Our study involved utilizing first principle calculations based on DFT to estimate the structural, electronic, and optical properties of Delafossite semiconductor in their tetragonal phases, namely $PdAlO_2$, $PdCrO_2$, and $PdRhO_2$. Our investigation showed that these three compounds, especially $PdCrO_2$, have favorable cohesive energies and display similar semiconductor behavior while having differing energy gaps. Furthermore, our investigation of their optical properties demonstrated that all three compounds exhibit favorable optical behavior, with $PdAlO_2$ displaying the highest absorption coefficient among the compounds. Overall, our findings provide valuable insights into the properties of these Delafossite semiconductors and their potential for use in various applications. Based on the results we obtained, we can conclude that $PdBO_2$ (B = Al, Cr and Rh) show promising potential for use in electro-optical fields and their applications, as their thermodynamic and electronic properties are favorable. Our findings also suggest that $PdAlO_2$ and $PdCrO_2$ may be suitable for use as thermoelectric materials, given their specific features, which were validated through the estimation of their thermoelectric properties using the semi-classical Boltzmann theory. Furthermore, we observed that $PdBO_2$ with an (Al) atom exhibits lower energy absorption ability and other thermal properties compared to the other compounds, indicating that it may be as suitable for use in photovoltaic applications. However, overall, our results agree with other theoretical studies, further supporting the potential use of these compounds in various applications.

Author contributions MEK: Conceptualization, Methodology, Formal analysis, Writing and Investigation; SSE: Verification, Supervision, Visualization, Conceptualization. Writing, SAA: Verification, Supervision, Visualization and Writing; AYA-R: Supervision, Visualization; AAM: Verification, Supervision; AM: Supervision, Visualization.

Funding No funding was received to assist with the preparation of this manuscript.

Data availability All the associated data with this study is present in the manuscript.

Declarations

Ethical approval There is no ethical approval required for this research work.

Competing interests There is no conflict of interest.

References

Abdelhamid, H.N.: Delafossite nanoparticle as new functional materials: advances in energy. Nanomed. Environ. Appl. Mater. Sci. Forum. **832**, 28–53 (2015). https://doi.org/10.4028/www.scientific.net/MSF.832.28

Akin, S., Sadegh, F., Turan, S., Sonmezoglu, S.: Inorganic $CuFeO_2$ delafossite nanoparticles as effective hole transport materials for highly efficient and long-term stable perovskite solar cells. ACS Appl. Mater. Interfaces. **11**, 45142–45149 (2019). https://doi.org/10.1021/acsami.9b14740

Ali, M.A., Khan, A., Khan, S.H., Ouahrani, T., Murtaza, G., Khenata, R., Omran, S.B.: First principles study of Cu based delafossite transparent conducting oxides $CuXO_2$ (X= Al, Ga, In, B, La, Sc, Y). Mater. Sci. Semicond. Process. **38**, 57–66 (2015)

Ali, M.A., Ullah, R., Dar, S.A., Murtaza, G., Khan, A., Mahmood, A.: Modeling of structural, elastic, mechanical, acoustical, electronic and thermodynamic properties of XPdF3 (X = Rb, Tl) perovskites

through density functional theory. Phys. Scr. **95**, 075705 (2020). https://doi.org/10.1088/1402-4896/ab8eee

Ali, M.A., Dar, S.A., AlObaid, A.A., Al-Muhimeed, T.I., Hegazy, H.H., Nazir, G., Murtaza, G.: Appealing perspectives of structural, electronic, mechanical, and thermoelectric properties of Tl_2(Se, Te)Cl_6 vacancy-ordered double perovskites. J. Phys. Chem. Solids. **159**, 110258 (2021a). https://doi.org/10.1016/j.jpcs.2021.110258

Ali, M.A., Alshahrani, T., Murtaza, G.: Defective perovskites Cs_2SeCl_6 and Cs_2TeCl_6 as novel high temperature potential thermoelectric materials. Mater. Sci. Semicond. Process. **127**, 105728–10557 (2021b). https://doi.org/10.1016/j.mssp.2021.105728

Al-Reyahi, A.Y., Al Azar, S., Mousa, A.A., Essaoud, S.S., Maghrabi, M., Berarma, K., Aqili, A., Mufleh, A., Radwan, H.I.A.: Investigation of electronic, optical, and thermoelectric properties of half-metallic spinel X_2NO_4 (X= B, Al): first-principles calculations. Comput. Condens. Matter. **98**, e00787–e00797 (2023)

Ambrosch-Draxl, C., Sofo, J.O.: Linear optical properties of solids within the full-potential linearized augmented planewave method. Comput. phys. commun. **175.1**, 1–14 (2006)

Becke, A.D., Johnson, E.R.: A simple effective potential for exchange. J. Chem. Phys. **124**, 221101–221105 (2006). https://doi.org/10.1063/1.2213970

Blaha, P., Schwarz, K., Tran, F., Laskowski, R., Madsen, G.K., Marks, L.D.: WIEN2k: an APW+ lo program for calculating the properties of solids. J. Chem. Phys. **152**, 074101–074131 (2020)

Broyden, C.G.: The convergence of a class of double-rank minimization algorithms 1. General considerations. IMA J. Appl. Math. **6**, 76–90 (1970a). https://doi.org/10.1093/imamat/6.1.76

Broyden, C.G.: The convergence of a class of double-rank minimization algorithms: 2. The new algorithm. IMA J. Appl. Math. **6**, 222–231 (1970b). https://doi.org/10.1093/imamat/6.3.222

Chadwick, A.V., Blacklocks, A.N., Rougier, A., Yaicle, C.: A structural study of delafossite-type $CuInO_2$ thin films. J. Phys. Conf. Ser. **249**, 012045–012057 (2010). https://doi.org/10.1088/1742-6596/249/1/012045

Gajdoš, M., Hummer, K., Kresse, G., Furthmüller, J., Bechstedt, F.: Linear optical properties in the projector-augmented wave methodology. Phys. Rev. B. **73**, 045112–045121 (2006). https://doi.org/10.1103/PhysRevB.73.045112

Gillispie, M.A.: Metal oxide-based transparent conducting oxides(Book). Doctor of Philosophy, Iowa State University, Digital Repository (2006). https://doi.org/10.31274/rtd-180813-16475

Hanaor, D.A.H., Sorrell, C.C.: Review of the anatase to rutile phase transformation. J. Mater. Sci. **46**, 855–874 (2011). https://doi.org/10.1007/s10853-010-5113-0

Kataria, S., Mudila, H., Kumar, A., Prasher, P.: Optical properties of novel materials for optoelectronic applications. Nanosci. Nanotechnol. Asia. **12**, 48–57 (2022). https://doi.org/10.2174/2210681213666221031103157

Khan, M.A., Kashyap, A., Solanki, A.K., Nautiyal, T., Auluck, S.: Interband optical properties of Ni_3Al. Phys. Rev. b. **48**, 16974–16979 (1993)

Kushwaha, P., Borrmann, H., Khim, S., Rosner, H., Moll, P.J.W., Sokolov, D.A., Sunko, V., Grin, Y., Mackenzie, A.P.: Single crystal growth, structure, and electronic properties of metallic delafossite $PdRhO_2$. Cryst. Growth Des. **17**, 4144–4150 (2017)

Madsen, G.K.H., Singh, D.J.: BoltzTraP. A code for calculating band-structure dependent quantities. Comput. Phys. Commun. **175**, 67–71 (2006). https://doi.org/10.1016/j.cpc.2006.03.007

Mm. Petit, Dulong: XLIV. Researches on some important points of the theory of heat. Philos. Mag. **54:**267–275 (1819). https://doi.org/10.1080/14786441908652225

Moreira, M., Afonso, J., Crepelliere, J., Lenoble, D., Lunca-Popa, P.: A review on the p-type transparent Cu–Cr–O delafossite materials. J. Mater. Sci. **57**, 3114–3142 (2022). https://doi.org/10.1007/s10853-021-06815-z

Mousa, A.A., Al-Azar, S.M., Essaoud, S.S., Berarma, K., Awad, A., Mahmoud, N.T., Jaradat, E.K., Abu-Jafar, M.S.: Structural, Elastic, Electronic, Magnetic, and Thermoelectric Characteristics of $MgEu_2X_4$ (X= S, Se) Spinel Compounds: Ab-Initio Calculations. Phys. Status Solidi B **259**, 2200191–2200205 (2022)

Murnaghan, F.D.: The compressibility of media under extreme pressures. Proc. Natl. Acad. Sci. **30**, 244–247 (1944). https://doi.org/10.1073/pnas.30.9.244

Otero-de-la-Roza, A., Luaña, V.: Gibbs2: A new version of the quasi-harmonic model code. I. Robust treatment of the static data. Comput. Phys. Commun. **182**, 1708–1720 (2011). https://doi.org/10.1016/j.cpc.2011.04.016

Otero-de-la-Roza, A., Abbasi-Pérez, D., Luaña, V.: Gibbs2: a new version of the quasiharmonic model code. II. Models for solid-state thermodynamics, features and implementation. Comput. Phys. Commun. **182**, 2232–2248 (2011). https://doi.org/10.1016/j.cpc.2011.05.009

Perdew, J.P., Burke, K., Ernzerhof, M.: Generalized gradient approximation made simple. Phys. Rev. Lett. **77**, 3865–3868 (1996). https://doi.org/10.1103/PhysRevLett.77.3865

Sâad Essaoud, S., Bouhemadou, A., Maabed, S., Bin-Omran, S., Khenata, R.: Pressure dependence of the electronic, optical, thermoelectric, thermodynamic properties of CsVO3: first-principles study. Philos. Mag. **102**, 1522–1546 (2022). https://doi.org/10.1080/14786435.2022.2057611

Sâad-Essaoud, S., Al Azar, S.M., Mousa, A.A., Al-Reyahi, A.Y.: DFT-Based investigation of electronic-structure, magnetic and thermoelectric properties of Dy_2CoMnO_6 double perovskite. Phys. Scr. **98**, 075930–75944 (2023a). https://doi.org/10.1088/1402-4896/acdd2c

Sâad-Essaoud, S., Bouhemadou, A., Ketfi, M.E., Allali, D., Bin-Omran, S.: Structural parameters, electronic structure and linear optical functions of $LuXCo_2Sb_2$ (X = V, Nb and Ta) double half Heusler alloys. Phys. B Condens. Matter. **657**, 414809–414819 (2023b). https://doi.org/10.1016/j.physb.2023.414809

Sâad-Essaoud, S., Al-Azar, S.M., Mousa, A.A., Masharfe, R.S.: Characterization of structural, dynamic, optoelectronic, thermodynamic, mechanical and thermoelectric properties of $AMgF_3$ (A = K or Ag) fluoro-perovskites compounds. Phys. Scr. **98**, 035820–035841 (2023c). https://doi.org/10.1088/1402-4896/acb6c0

Shi, L.-J., Fang, Z.-J., Li, J.: First-principles study of p-type transparent conductive oxides $CuXO_2$ (X=Y, Sc, and Al). J. Appl. Phys. **104**, 073527–073532 (2008). https://doi.org/10.1063/1.2991157

Shi, J., Cerqueira, T.F.T., Cui, W., Nogueira, F., Botti, S., Marques, M.A.L.: High-throughput search of ternary chalcogenides for p-type transparent electrodes. Sci. Rep. **7**, 43179–43192 (2017). https://doi.org/10.1038/srep43179

Singh, S., Tangra, A.K., Lotey, G.S.: Optical and Luminescence Properties of β-$NaFeO_2$ Nanoparticles. Electron. Mater. Lett. **14**, 594–598 (2018). https://doi.org/10.1007/s13391-018-0067-5

Slack, G.A.: Nonmetallic crystals with high thermal conductivity. J. Phys. Chem. Solids. **34**, 321–335 (1973)

Telfah, A., Sâad Essaoud, S., Baaziz, H., Charifi, Z., Alsaad, A.M., Ahmad, M.J.A., Hergenröder, R., Sabirianov, R.: Density functional theory investigation of physical properties of KCrZ (Z= S, Se, Te) half-Heusler alloys. Phys. Status Solidi B. **258**, 2100039–2100057 (2021)

Ul Haq, B., AlFaify, S., Jbara, A.S., Ahmed, R., Butt, F.K., Laref, A., Chaudhry, A.R., Shah, Z.A.: Optoelectronic properties of three PbSe polymorphs. Ceram. Int. **46**, 22181–22188 (2020). https://doi.org/10.1016/j.ceramint.2020.05.295

Woods-Robinson, R., Han, Y., Zhang, H., Ablekim, T., Khan, I., Persson, K., Zakutayev, A.: Wide band gap chalcogenide semiconductors. Chem. Rev. **120**, 4007–4055 (2020). https://doi.org/10.1021/acs.chemrev.9b00600

Zhang, T., Wu, M.-Y., Yan, D.-Y., Mao, J., Liu, H., Hu, W.-B., Du, X.-W., Ling, T., Qiao, S.-Z.: Engineering oxygen vacancy on NiO nanorod arrays for alkaline hydrogen evolution. Nano Energy **43**, 103–109 (2018). https://doi.org/10.1016/j.nanoen.2017.11.015

Zhang, N., Sun, J., Gong, H.: Transparent p-Type semiconductors: copper-based oxides and oxychalcogenides. Coatings **9**, 137–164 (2019). https://doi.org/10.3390/coatings9020137

Authors and Affiliations

Mohammed Elamin Ketfi[1] · Saber Saad Essaoud[2,3] · Said Al Azar[4] · Anas Y. Al-Reyahi[5] · Ahmad A. Mousa[6,7] · Ahmad Mufleh[8]

✉ Mohammed Elamin Ketfi
mohammedelamin.ketfi@univ-msila.dz

Saber Saad Essaoud
saber.saadessaoud@univ-msila.dz

Said Al Azar
q_saed74@yahoo.com

Anas Y. Al-Reyahi
anasy@hu.edu.jo

Ahmad A. Mousa
amousa@meu.edu.jo

Ahmad Mufleh
Ahmad_mufleh@yahoo.com

[1] Department of Electronics, Faculty of Technology, University of M'sila, 28000 M'sila, Algeria

[2] Department of Physics, Faculty of Science, University of M'sila, 28000 M'sila, Algeria

[3] Laboratoire de Physique des Particules et Physique Statistique, Ecole Normale Supérieure-Kouba, BP 92, 16050 Vieux-Kouba, Algiers, Algeria

[4] Department of Physics, Faculty of Science, Zarqa University, Zarqa 13132, Jordan

[5] Department of Physics, Faculty of Science, The Hashemite University, P. O. Box 330127, Zarqa 13133, Jordan

[6] Department of Basic Sciences, Middle East University, Amman 11831, Jordan

[7] Applied Science Research Center, Applied Science Private University, Amman, Jordan

[8] Preparatory Deanship, Prince Sattam Bin Abdulaziz University, Al-Kharj, Saudi Arabia